

# High Resolution Mid-Infrared Imaging of the Nucleus of NGC 1068

J. J. Bock, K. A. Marsh, M. E. Ressler, and M. W. Werner

Jet Propulsion Laboratory, 4800 Oak Grove Drive, Pasadena, CA 91109

Received 21 January 1998;    accepted 29 June 1998

## ABSTRACT

We have obtained mid-infrared images of the nucleus of NGC 1068 from the Hale 5 m telescope at Mt. Palomar with diffraction-limited resolution and high sensitivity at  $\lambda = 8.8, 10.3,$  and  $12.5 \mu\text{m}$ . Deconvolved images show that the infrared emission extends north to south in the inner  $2''$ , consisting of a central peak, a component extending  $1''$  north of the central source, a component extending  $1''$  south of the central source, and several smaller structures located  $1''$  to the northeast. The central peak is extended  $0.4''$  N-S and unresolved ( $\leq 0.2''$ ) E-W. We find that  $50 \pm 5\%$  of the flux emerges from the central  $0.4''$  and that a single unresolved point source can account for only  $27 \pm 5\%$  of the total flux. However, if the central peak arises from optically thick emission, we estimate that the emitting region has a projected area  $\geq 2 \text{ pc}^2$ , and may thus contain a compact source such as a parsec-scale torus. We observe a correspondence between the northern extension and the northeastern sources appearing on the mid-infrared images and the [OIII] clouds A-C & E. We interpret the faint optical counterpart to the mid-infrared southern extension as being due to partial obscuration by the intervening disk of the host galaxy. The N-S extension of the mid-infrared emission coincides with one wall of the conical narrow line region and aligns with the N-S orientation of the radio jet close to the nucleus. We interpret the infrared emission as arising from optically thick dust lining the walls of the low density cavity formed by the radio jet and heated by radiation from the central source.

*Subject headings:* galaxies: active, Seyfert — infrared: galaxies

## 1. Introduction

NGC 1068 represents the closest example of a Seyfert 2 galaxy ( $D=14$  Mpc assuming  $H_0 = 75 \text{ km s}^{-1} \text{ Mpc}^{-1}$ ,  $68 \text{ pc/arcsec}$ ) and is thus amenable to study with high resolution imaging. The characteristic smooth optical continuum and broad optical line emission associated with a Seyfert 1 galaxy can be seen in polarized light (Antonucci & Miller 1985), leading to the interpretation that NGC 1068 harbors an obscured Seyfert 1 nucleus. The absence of strong X-ray emission (Mulchaey, Mushotzky, & Weaver 1992) indicates that the nucleus is obscured by a column density of gas in excess of  $10^{24} \text{ cm}^{-2}$ .

The obscuring medium which prevents direct observation of the Seyfert 1 nucleus has an undetermined morphology and may consist of a parsec-scale torus (Antonucci 1993). A compact torus would allow a direct view of the nucleus when viewed pole-on as in the case of a Seyfert 1 galaxy, but an obscured view when viewed edge-on as in the case of a Seyfert 2 galaxy, and would naturally explain the conical morphology of the narrow-line region (NLR) observed in NGC 1068 and many other Seyfert galaxies (Mulchaey, Wilson, & Tsvetanov 1996). Recently, interferometric radio observations of water masers in the nucleus of NGC 1068 (Gallimore et al. 1996a; Greenhill et al. 1996) indicate the presence of molecular material as close as  $0.4 \text{ pc}$  to the purported nucleus with Keplerian rotational kinematics.

Mid-infrared observations allow high-resolution, relatively unobscured imaging of the nucleus of NGC 1068 at the peak of its SED (Roche et al. 1991). Previous mid-infrared observations (Braatz et al. 1993) resolved approximately half the emission into a spatially extended component. Cameron et al. (1993) proposed that the central source is instead obscured by a large envelope of clumpy molecular material surrounding the nucleus, and that the extended mid-infrared emission originates from molecular clouds exposed to radiation from the concealed Seyfert 1 nucleus. The morphology of the material obscuring

the nucleus of NGC 1068 is thus uncertain and may be more complex than a simple torus.

## 2. Observations

We conducted observations from the Cassegrain focus of the 5 m Hale telescope on Mt. Palomar on the nights of 1995 December 3-4 using MIRLIN, a new mid-infrared broadband camera developed at JPL (Ressler et al., 1994) based on the HF-16 128×128 Si:As BIB array fabricated by Boeing (formerly Rockwell). The large well depth of  $3 \times 10^7$  e<sup>-</sup>/pixel makes the detector particularly well-suited for use under the large photon backgrounds encountered in broadband ground-based mid-infrared astronomy. Twin filter wheels allow the observer to select a wide array of filters, including a narrow-band CVF, for observations in the spectral band 5  $\mu$ m - 26  $\mu$ m. We selected 3 bands within the N-band atmospheric window with moderate bandwidth ( $\Delta\lambda/\lambda = 10\%$ ), centered at  $\lambda = 8.8, 10.3,$  and  $12.5 \mu$ m, for our observations of NGC 1068. Although MIRLIN is somewhat more sensitive observing with a broadband N filter, we chose the narrower bands to probe the depth of the 10  $\mu$ m dust silicate feature. We used a plate scale of 0.15'' pixel<sup>-1</sup> to obtain fully sampled images.

The target was observed in a standard “chop-nod” scheme to remove the foreground emission from the telescope and the atmosphere. We typically chopped at 1.25 Hz, coadding several 50 - 100 ms integrations at each mirror position to obtain on and off beam exposures A and B. After 20 s the telescope was nodded to obtain 2 further exposures C and D. The observation cycle was repeated multiple times, dithering the position of the telescope several arc seconds after each cycle in order to sample different pixels on the detector. We obtain a single background-subtracted image by accurately registering each group of exposures (A<sub>*i*</sub>-B<sub>*i*</sub>)-(C<sub>*i*</sub>-D<sub>*i*</sub>) using the bright nucleus of NGC 1068 and then coadding,  $\Sigma_i [(A_i-B_i)-(C_i-D_i)]$ .

The results reported in this paper are derived from the data obtained on 3 December with a small chop and nod throw (both  $10''$ ) in order to keep the nucleus on the array at all times and to realize maximum sensitivity on the compact nucleus. Observations on 4 December were obtained with a  $20''$  throw and confirmed that extended emission around the nucleus is sufficiently compact as to not appreciably alter the results obtained with the  $10''$  throw.

During the night of 3 December we observed, in sequential order over 2.5 hours,  $\beta$  Andromedae (AM = 1.1), NGC 1068 (1.6),  $\beta$  And (1.0), NGC 1068 (1.35),  $\beta$  And (1.0), and  $\alpha$  Tauri (1.4) in each of the 3 wavelength bands. The measured flux of NGC 1068 and the reference stars were stable within each observation, showing  $< 5\%$  fluctuations between exposures due to variations in atmospheric transparency. Unfortunately, the appreciable (20%) change in flux between the two observations of NGC 1068 and the discrepancy in the cross-calibration of the reference stars indicate that weather conditions were not suitable for accurate photometry.

### 3. Analysis

The raw images of NGC 1068, displayed with logarithmic contours in Fig. 1, represent a signal-to-noise ratio in total flux in excess of  $10^3$  and a peak signal in excess of  $10^2$  times the per pixel noise level, where the noise is estimated from the off-source data. The raw images of  $\alpha$  Tau display the lobed diffraction pattern with  $0.5''$  width (FWHM) characteristic of the 5 m Hale telescope and have a signal-to-noise ratio in total flux greater than  $10^4$ .

EDITOR: PLACE FIGURE 1 HERE.

### 3.1. Deconvolution

The mid-infrared images are deconvolved using a technique developed by Richardson & Marsh (1983) (also see Marsh et al. 1995) which yields the most probable image based on the assumptions of Gaussian prior statistics with positivity in the pre-convolved image and measurement noise statistics described by a Gaussian with zero mean. We obtain qualitatively similar results by instead deconvolving our images using a maximum likelihood routine.

The deconvolved image depends critically on the quality and stability of the PSF. The multiple observations of  $\beta$  And serve to monitor any changes in the PSF due to atmospheric fluctuations or drifts in the focus of the telescope. Because  $\alpha$  Tau is matched in air mass to NGC 1068 during the observations, we selected it for the PSF in the deconvolution shown in Fig. 1. We can test the stability of the PSF during the observations by deconvolving the raw image of NGC 1068 using the PSF from  $\beta$  And instead of  $\alpha$  Tau, and obtain similar results. We can also deconvolve the image of  $\beta$  And using the PSF from  $\alpha$  Tau, resulting in a compact image with  $\sim 0.2''$  width (FWHM) as shown in Fig. 1.

The deconvolved images of NGC 1068 show a central peak, and resolve structure elongated roughly N-S. These data are in general accord with the deconvolved images reported by Braatz et al. (1993), with  $\sim 0.7''$  resolution (FWHM) after deconvolution, which resolve emission extended NE-SW. With higher angular resolution our data show that the resolved emission closer to the nucleus extends N-S, as is clearly evident in the raw images of NGC 1068 (FWHM =  $0.5''$ ) and in the inner contours of the Braatz et al. (1993) image. The flux of the central region, obtained by locating a  $0.4''$  diameter false aperture on the peak, accounts for  $50 \pm 5\%$  of the measured brightness in these images, consistent with the result of 54% from Braatz et al. (1993). Reconvolving the deconvolved images with a  $0.7''$  FWHM Gaussian beam, we obtain good agreement with the Braatz et al. (1993) data.

Resolved structures located to the northeast of the central peak are evident at each of the three wavelengths. Because these structures have low surface brightness, on order of 2% of the peak brightness, their position and flux are more sensitive to variations in the PSF. Nevertheless, the northeastern structures appear with a roughly hook-like geometry in all three wavelength bands, and are even evident in data (from other nights) rejected for poor atmospheric stability if deconvolved. Therefore we believe that the northeastern structures are not an artifact of the deconvolution.

In our deconvolved images we find that the central peak consists of a structure with width  $\sim 0.2''$  (FWHM) E-W and width  $\sim 0.4''$  (FWHM) N-S. Because the width in the E-W direction is similar to that of the deconvolved image of  $\beta$  And ( $0.2''$  FWHM), we consider the central peak to still be unresolved E-W. We can estimate the flux from the unresolved component by assuming that the deconvolved PSF is a symmetric Gaussian with width  $0.2''$ . If we extract an unresolved point source located at the peak, it accounts for  $27 \pm 5\%$  of the total emission. The N-S extension of the central peak is better described, however, by an unresolved  $0.4''$  uniform line source accounting for  $55 \pm 5\%$  of the total emission. Thus at least 73% of the total flux is resolved N-S in the deconvolved images.

If the mid-infrared peak contained a significant contribution from a point source which was partially obscured by dust, one might expect that the point source would differ spectrally from the surrounding emission in the  $10 \mu\text{m}$  silicate feature. However, the SED of the extracted point source and the SED of the residual flux in the central  $0.4''$  agree to within 10%. This is consistent with the large column density of obscuring material inferred from X-ray measurements blocking a direct view of the purported Seyfert 1 nucleus. We note that the near-infrared point source observed by Thatte et al. (1997), extrapolating to mid-infrared wavelengths, contributes only a small fraction ( $0.2 - 10\%$ ) of the total nuclear flux.

Although weather conditions were not suitable for absolute photometry, we can probe the depth of the 10  $\mu\text{m}$  silicate feature. The measured  $\lambda F_\lambda(8.5 \mu\text{m}) / \lambda F_\lambda(10.3 \mu\text{m})$  and  $\lambda F_\lambda(8.5 \mu\text{m}) / \lambda F_\lambda(12.5 \mu\text{m})$  flux ratios for the entire nucleus agree with Roche et al. (1991) to within 10 % based on the calibration obtained with  $\alpha$  Tau. We find that the silicate feature is weak throughout the image, being most pronounced at the mid-infrared peak where  $\lambda F_\lambda(10.3 \mu\text{m}) / 0.5[\lambda F_\lambda(8.5 \mu\text{m}) + \lambda F_\lambda(12.5 \mu\text{m})] = 0.8$ .

### 3.2. Location of the Nucleus

In Fig. 2 we compare the deconvolved 12.5  $\mu\text{m}$  mid-infrared image with the NLR imaged in the  $\lambda 5007 \text{ \AA}$  emission line of [OIII] with  $0.05''$  resolution using the corrected Hubble Space Telescope (Macchetto et al. 1994). Because we did not obtain accurate astrometry of the mid-infrared images, we place the peak of our deconvolved mid-infrared image at the location of the mid-infrared peak determined by Braatz et al. (1993). The [OIII] map shows clumpy emission in a roughly conical region extended NE whereas the mid-infrared emission is elongated N-S. We note the correspondence between the infrared northern extension and the [OIII] clouds A-C & E. Although the positions of the NE sources are not well determined, the hook-like NE feature may coincide with the [OIII] clouds D and F. Given the limitations of the astrometry, we cannot discern if the northern extension coincides with the peaks of the [OIII] clouds A-C & E, or is displaced to the west by  $\sim 0.15''$ . The central peak and southern extension in the mid-infrared emission do not have distinct counterparts in the [OIII] map. The northern extension appears to trace the western wall, and the southern extension the eastern wall, of the conical NLR (Pogge 1989). With the exception of the weak northeastern sources, mid-infrared emission is largely absent from the conical region itself.

High resolution radio maps of the nucleus of NGC 1068 resolve 4 distinct sources



and a collimated bipolar jet (Ulvestad, Neff, & Wilson 1987). A comparison between the mid-infrared emission and a 5 GHz map of the radio continuum (Gallimore, Baum, & O’Dea 1996b) (see Fig. 3), shows that the N-S extension of the mid-infrared emission aligns with the N-S orientation of the radio jet close to the nucleus.

#### 4. Discussion

The copious infrared nuclear emission of NGC 1068 ( $L \sim 10^{11}L_{\odot}$ ), originates from thermal dust emission extending out to  $\sim 70$  pc. The emission is associated with a gas mass of at least  $M > m_H[F_{\nu}/B_{\nu}(T)]D^2(10^{23}cm^{-2}) = 10^4M_{\odot}$ . Several mechanisms have been proposed to heat the dust (radiation from a Seyfert 1 nucleus, star forming regions, shocks). Tresch-Fienberg et al. (1987) propose that the northeastern sources might arise from star formation. In addition to a lack of evidence for significant star formation near the nucleus (Cameron et al. 1993), we find that at higher resolution the northeastern sources contain only a small fraction ( $\sim 10\%$ ) of the total flux. The nuclear stellar core observed in K-band imaging to extend out to  $2.5''$  contributes a minority of the total nuclear luminosity unless the stars are very young ( $< 10^7$  years old, Thatte et al. 1997). Capetti, Axon, & Macchetto (1997a) suggest that shocks may explain the ionization structure observed in optical line emission. Unfortunately, the location of these shock fronts are  $4''$  from the nucleus and outside of the central region we image in the mid-infrared. Furthermore, shocks fail to provide sufficient energy to explain the observed mid-infrared flux in the central region (Cameron et al. 1993). Radiation from a Seyfert 1 nucleus alone is sufficient to supply the necessary luminosity and can heat dust out to large distances (Braatz et al. 1993).

The lack of a strong silicate feature might be explained by depletion of silicates; however, the estimated dust temperature ( $T \simeq 350$  K, Tresch-Fienberg et al. 1987) is far below the expected sublimation temperature of silicate grains (Laor & Draine 1993). An

arrangement of optically thin dust in emission and absorption could be invoked to explain the weakness of the silicate feature, but seems unlikely to hold over the entire image, including the partially obscured southern extension (see below). Thus we conclude the most likely explanation is that the infrared emission arises from optically thick dust.

#### 4.1. Northern Extension

To the north of the nucleus, the mid-infrared emission corresponds to the peaks (clouds A-F) in the more extended [OIII] emission. Braatz et al. (1993) proposed that the extended mid-infrared emission originates from dust associated with the low density NLR. However, if the mid-infrared emission arises from optically thick dust, the mid-infrared emitting regions ( $A_V \geq 20$ ) must be physically distinct from the optically thin ( $A_V \sim 1.5$ ) NLR. The mid-infrared emission may originate from dust deep within clumpy molecular clouds, and the [OIII] emission from the envelope of these clouds, giving a correspondence between the mid-infrared and [OIII] emission where the surfaces of the clouds are relatively unobscured.

The beam filling factor of the extended mid-infrared emission may be calculated by relating the observed surface brightness to that of a blackbody,  $f = \tau f_A = I_\nu/B_\nu(T)$ , where  $f_A$  is the areal filling factor and  $\tau$  is the optical depth. Assuming  $T = 350$  K we obtain  $f \simeq 3 \times 10^{-3}$  for the northern and southern extensions, much smaller than the areal filling factor of the ionized [OIII] emitting gas,  $f_A = 0.1$  (Netzer 1990). Interestingly, the volume filling factor of the extended molecular gas envelope is  $f_V < 10^{-3}$  (Rotaciuc et al. 1991), suggesting that the mid-infrared emission may correspond to a heated subsection of the thick ( $N \sim 10^{23} \text{ cm}^{-2}$ ) molecular material surrounding the nucleus (Blietz et al. 1994; Planesas, Scoville, & Myers 1991).

## 4.2. Southern Extension

The southern mid-infrared extension does not appear to have a clear optical NLR counterpart, although some structure is notable in the [OIII] map to the south of the nucleus. A modest quantity of dust in the intervening disk of the host galaxy may obscure the [OIII] emission from the southern cone, and indeed a clearer view of the southern counter-cone may be obtained in polarized near-infrared images (Packham et al. 1997). We note that the [OIII] to mid-infrared ratio is 5 times weaker along the southern extension than the northern extension, giving an obscuration of  $A_V = 1.7$  if the northern extension and southern extension are under similar physical conditions. This estimate is in general agreement with the column density of gas,  $N_H \sim 2 \times 10^{21} \text{cm}^{-2}$ , estimated by Macchetto et al. (1994) based on the reddening of the southern lobe. We note that asymmetry in the northern and southern brightness observed in the radio (see Fig. 3) also holds in the mid-infrared as the northern extension appears to be approximately twice as luminous as the southern extension.

## 4.3. Unresolved Component

We can estimate the projected area of the emission in the central region with a simple blackbody argument if the emission is optically thick,  $A = D^2 F_\nu / B_\nu(T)$ , assuming  $D = 14$  Mpc is the distance to NGC 1068 and  $T = 350$  K. Including the entire flux from the central  $0.4''$ , which is well described by a line source, we find that the emitting area is  $4 \text{ pc}^2$ . Assuming the flux obtained by removing a point source at the central peak (see section 3.1), the emitting area is  $2 \text{ pc}^2$ . Thus the mid-infrared peak may harbor a compact source, such as a parsec-scale dusty torus. If the emission is obscured by intervening dust or is optically thin however, the source size will be underestimated (although the weakness of the silicate feature throughout the image suggests that these effects are small). If the

central source consists of emission from regions of dust at several different temperatures, partially obscured by cooler dust (e.g. Pier & Krolik 1992; Efstathiou, Hough, & Young 1995; Heisler, Lumsden, & Bailey 1997), the spectrum and effective size of the central source are model dependent.

#### 4.4. Morphology

If the mid-infrared emission is indeed powered by radiation from the central source, then its morphology denotes regions where radiation from the central source is absorbed by dust and converted to thermal infrared radiation. Some of the energy actually may be reradiated first by hot ( $T \sim 1000K$ ) dust close to the central source. However, the relatively low inferred bolometric luminosity of the K-band point source observed by Thatte et al. (1997) in NGC 1068 and the lack of prominent near-infrared emission in the SED's of Seyfert 1 and 2 galaxies (Roche et al. 1991; Mas-Hesse et al. 1995) suggest that the fraction of reradiated energy is modest. Although a compact source may be located at the mid-infrared peak, these data indicate that of the majority of the radiation from the central source (not including the fraction which escapes completely) is actually absorbed at distances greater than 10 pc. Therefore lines of sight to the nucleus exist which are intercepted not by a compact torus but by dust located up to  $\sim 70$  pc from the nucleus.

As an alternative to a simple torus, we suggest that the morphology of the extended obscuring medium traced by the mid-infrared emission is related to the morphology of the radio jets. We observe that the mid-infrared emission in the central  $0.4''$  is elongated N-S following the N-S orientation of the radio jet closest to the nucleus. This suggests that the mid-infrared emission arises from clouds lining the walls of a low density cavity heated by radiation from the central source. The walls of the low density cavity may be an extension of the compact structure mapped in H<sub>2</sub>O maser emission with an opening angle

of  $\sim 90^\circ$  (Greenhill et al. 1996). The resolution of these deconvolved mid-infrared images is insufficient to distinguish if the emission in the central  $0.4''$  has a linear or conical shape. A compact torus may be responsible for preventing radiation propagating E-W, explaining the N-S morphology of the mid-infrared emission.

Further from the nucleus, the northern and southern extensions of the mid-infrared emission align along a single wall of the conical ionization region. Although the filling factor of the extensions is low, the data cannot distinguish whether the emission consists of a coherent linear structure extending N-S of the nucleus which is unresolved E-W, or if it breaks up into small unresolved clumps. We note that mid-infrared and [OIII] emission are absent at the northernmost radio source NE, as would be expected if the radio jet has swept out a cavity of ionized gas (Capetti et al. 1997b; Gallimore et al. 1996b). We also observe that the northern extension terminates approximately at the location where the radio jet bends eastward, near the radio component C where the radio jet may be diverted by a giant molecular cloud (Gallimore et al. 1996b).

## 5. Conclusions

These images resolve the majority of the mid-infrared emission in the nucleus of NGC 1068 and show that emission from a compact central source can only account for a fraction of the total flux. With improved spatial resolution we determine that the resolved structure extends N-S in the innermost regions, corresponding to the orientation of the radio jet, with separate structures located to the northeast of the central source. We interpret the mid-infrared emission as arising from optically thick dust extending out to  $\sim 70$  pc, associated with a gas mass  $M \geq 10^4 M_\odot$ , and heated by radiation from the central Seyfert 1 nucleus. In order to explain the observed mid-infrared morphology we postulate that dust lining the walls of a low-density cavity is heated by radiation from the central source.

The work described in this paper was carried out at the Jet Propulsion Laboratory, California Institute of Technology, under an agreement with the National Aeronautics and Space Administration. We acknowledge the support of the JPL Director’s Discretionary Fund and NASA’s Office of Space Science. Observations at the Palomar Observatory were made as part of a continuing collaborative agreement between Palomar Observatory and JPL. The authors thank the staff at Mt. Palomar for their assistance during the observations, J. F. Gallimore for providing the [OIII] and radio images, and David Seib for providing the focal plane array.

## REFERENCES

- Antonucci, R. R. J. 1993, *ARA&A*, 31, 473
- Antonucci, R. R. J., & Miller, J. S. 1985, *ApJ*, 297, 621
- Blietz, M., Cameron, M., Drapatz, S., Genzel, R. Krabbe, A., Van der Werf, P., Strenberg, A., & Ward, M. 1994, *ApJ*, 421, 92
- Braatz, J. A., Wilson, A. S., Gezari, D. Y., Varosi, F., & Beichman, C. A. 1993, *ApJ*, 409, L5
- Cameron, M., Storey, J. W., Rotaciuc, V., Genzel, R., Verstraete, L., Drapatz, S., Siebenmorgen, R., & Lee, T. J. 1993, *ApJ*, 419, 136
- Capetti, A., Axon, D. J., & Macchetto, F. D. 1997a, *ApJ*, 487, 560
- Capetti, A., Macchetto, F. D., & Lattanzi, M. G. 1997b, *ApJ*, 476, L67
- Efstathiou, A., Hough, J. H., & Young, S. 1995, *MNRAS*, 277, 1134.
- Evans, I. N., Ford, H. C., Kinney, A. L., Antonucci, R. R. J., Armus, L., & Caganoff, S. 1991, *ApJ*, 369, L27
- Gallimore, J. F., Baum, S. A., O’Dea, C. P., Brinks, E., & Pedlar, A. 1996a, *ApJ*, 462, 740
- Gallimore, J. F., Baum, S. A., & O’Dea, C. P. 1996b, *ApJ*, 464, 198
- Greenhill, L. J., Gwinn, C. R., Antonucci, R., & Barvainis, R. 1996, *ApJ*, 472, L21
- Heisler, C. A., Lumsden, S. L., & Bailey, J. A. 1997, *Nature*, 385, 700
- Laor, A., & Draine, B. T. 1993, *ApJ*, 402, 441

- Macchetto, F., Capetti, A., Sparks, W. B., Axon, D. J., & Boksenberg, A. 1994, *ApJ*, 435, L15
- Marsh, K. A., Van Cleve, J. E., Mahoney, M. J., Hayward, T. L., & Houck, J. R. 1995, *ApJ*, 451, 777
- Mas-Hesse, J. M., Rodriguez-Pascual, P. M., de Cordoba, L. S. F., Mirabel, I. F., Wamsteker, W., Makino, F., & Otani, C. 1995, *A&A*, 298, 22
- Mulchaey, J. S., Mushotzky, R. F., & Weaver, K. A. 1992, *ApJ*, 390, 69
- Mulchaey, J. S., Wilson, A. S., & Tsvetanov, Z. 1996, *ApJ*, 467, 197
- Netzer, H. 1990, in *Saas-Fée Advanced Course, Active Galactic Nuclei*, Vol. 20, ed. T. J. L. Courvoisier & M. Mayor (Berlin:Springer), 57
- Packham, C., Young, S., Hough, J. H., Axon, D. J., & Bailey, J. A. 1997, *MNRAS*, 288, 375
- Pier, E. A., & Krolik, J. H. 1992, *ApJ*, 401, 99.
- Planesas, P., Scoville, N., & Myers, S. T. 1991, *ApJ*, 369, 364
- Pogge, R. 1989, *ApJ*, 345, 730
- Ressler, M. E., Werner, M. W., Van Cleve, J., & Chou, H. A. 1994, in *Infrared Astronomy with Arrays: The Next Generation*, ed. I. S. McLean (Dordrecht:Kluwer), 429
- Richardson, J. M., & Marsh, K. A. 1983, *Proc. SPIE*, 413, 79
- Roche, P. F., Aitken, D. K., Smiyh, C. H., & Ward, M. J. 1991, *MNRAS*, 248, 606
- Rotaciuc, V., Krabbe, A., Cameron, M., Drapatz, S., Genzel, R., Sternberg, A., & Storey, J. W. V. 1991, *ApJ*, 370, L23
- Thatte, N., Quirrenbach, A., Genzel, R., Maiolino, R., & Tecza, M. 1997, *ApJ*, 490, 238



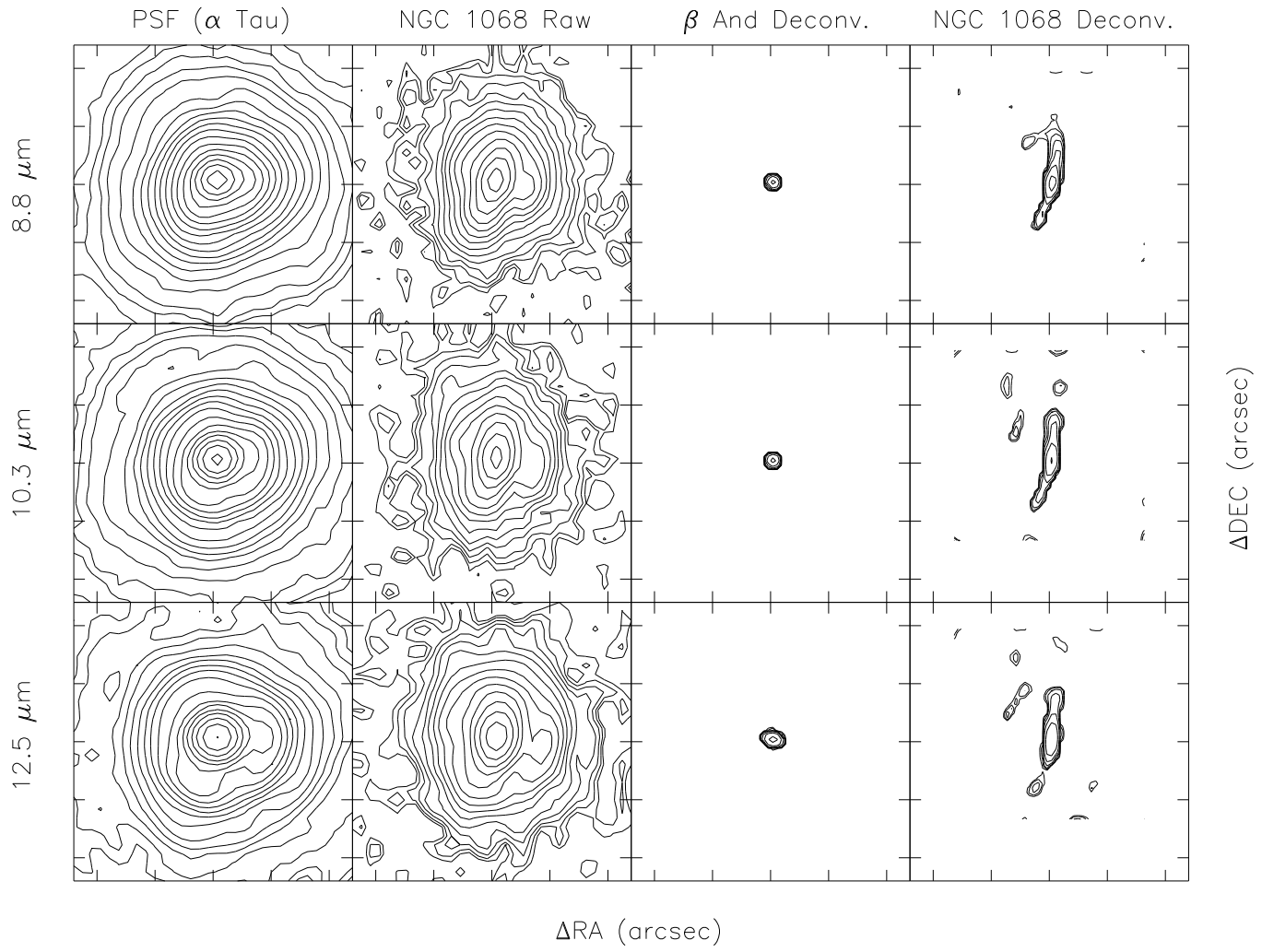
Tresch-Fienberg, R., Fazio, G. G., Gezari, D. Y., Hoffman, W. F., Lamb, G. M., Shu, P. K.,  
& McCreight, C. R. 1987, ApJ, 312, 5421

Ulvestad, J. S., Neff, S. G., & Wilson, A. S. 1987, AJ, 93, 22

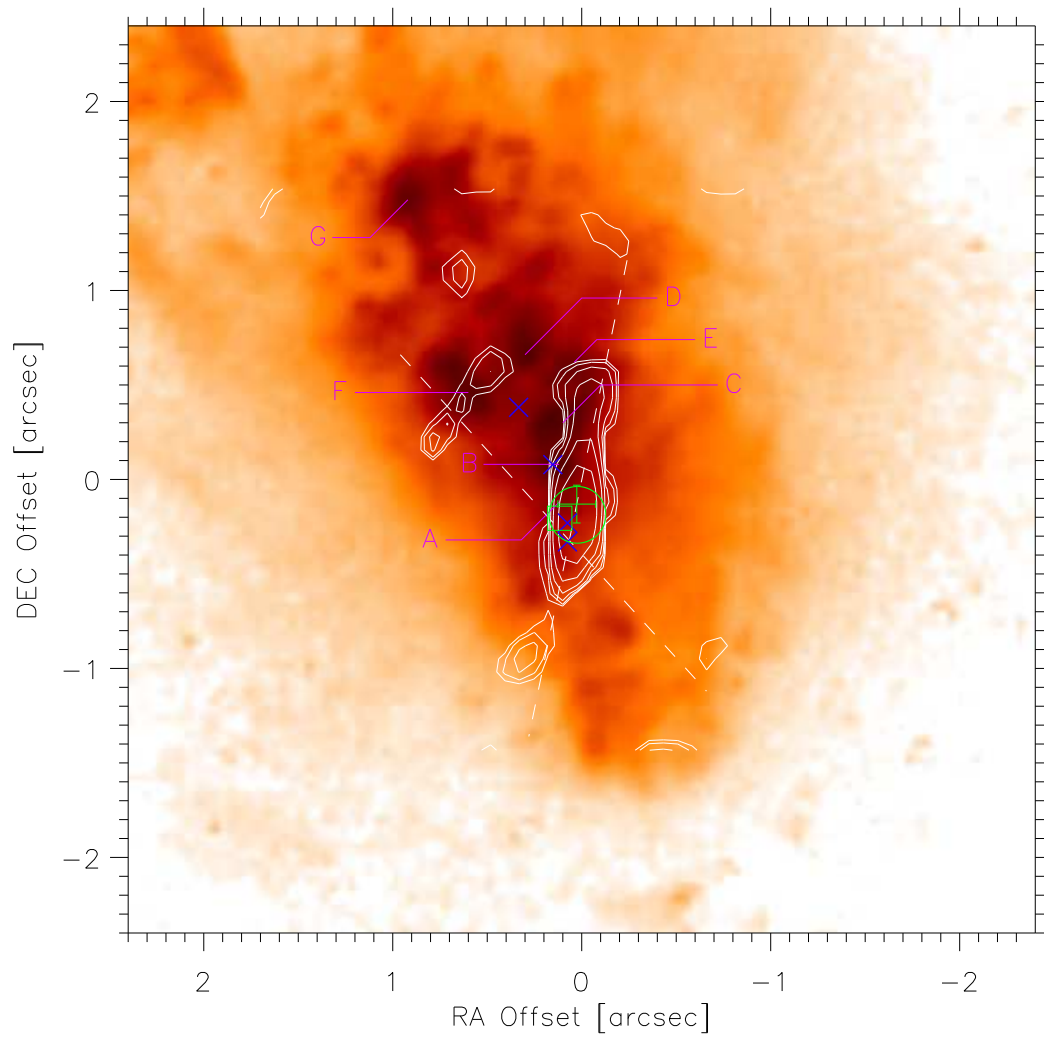
Fig. 1.— Panels from left to right show the raw image of  $\alpha$  Tau (PSF), the raw image of NGC 1068, the deconvolved image of  $\beta$  And using the PSF from  $\alpha$  Tau, and the deconvolved image of NGC 1068 using the PSF from  $\alpha$  Tau. Wavelength bands of observation are  $8.8 \mu\text{m}$  (top),  $10.3 \mu\text{m}$  (middle), and  $12.5 \mu\text{m}$  (bottom). For the raw images, contours begin at the  $1\sigma$  level  $\text{pixel}^{-1}$  and increase by multiplicative factors of  $\sqrt{2}$ . The deconvolved images have 8 contours beginning at 0.8 of the peak value and decreasing by multiplicative factors of 2. The field of view in each panel is  $4.8'' \times 4.8''$ .

Fig. 2.— Comparison of the deconvolved  $12.5 \mu\text{m}$  image with the [OIII]  $\lambda 5007 \text{ \AA}$  HST image of Macchetto et al. (1994). The contour spacing for the mid-infrared image is as in Fig. 1, and the [OIII] map is displayed with a logarithmic stretch. The letters label local maxima in the [OIII] emission as described by Evans et al. (1991). The green circle denotes the location of the mid-infrared peak determined by Braatz et al. (1993), the square denotes the location of the center of UV polarization (determined most recently by Capetti et al. 1997b), and the cross denotes the location of the near-IR peak determined by Thatte et al. (1997). Blue X's denote the location of the 4 radio peaks (S2, S1, C and NE from south to north) assuming the registration of Gallimore et al. (1996b). The water masers located at the S1 radio source trace out a velocity gradient which can be described as an edge-on Keplerian disk. The size of each green symbol is equal to the positional uncertainty quoted by the authors.

Fig. 3.— Comparison of the deconvolved  $12.5 \mu\text{m}$  image with the 5 GHz map of Gallimore et al. (1996b). We register the maps by simply aligning the mid-infrared peak with S1, consistent to within the error in registering the two images to the [OIII] map.



# Comparison of [OIII] and IR Images



Comparison of Radio and IR Images

